Inorg. Chem. **2004**, *43*, 2556–2563

Two-Dimensional Metallic Chain Compounds $Y_5M_2Te_2$ (M = Fe, Co, Ni) That Are Related to Gd_3MnI_3. The Hydride Derivative $Y_5Ni_2Te_2D_{0.4}$

Paul A. Maggard and John D. Corbett*

Department of Chemistry, Iowa State University, Ames, Iowa 50011

Received November 10, 2003

$Y_5M_2Te_2$ (M = Fe, Co, Ni) have been prepared by high-temperature solid-state techniques and shown to be isostructural and orthorhombic *Cmcm* (No. 63), $Z = 4$. The structure was established by single crystal X-ray methods at 23 °C for M = Fe, with $a = 3.9594(3)$ Å, $b = 15.057(1)$ Å, and $c = 15.216(1)$ Å. The new structure contains zigzag chains of the late transition metal sheathed by a column of yttrium atoms that are in turn condensed through trans vertices on the latter to yield 2D bimetallic layers separated by single layers of tellurium atoms. Reaction of hydrogen with $Y_5Ni_2Te_2$ causes a rumpling of the Y–Ni layers as determined by both single X-ray crystal means at 23 °C and neutron powder diffraction at −259 °C for $Y_5Ni_2Te_2D_{0.41(1)}$, *Pnma* (No. 62), $Z = 4$. Lattice constants from the former study are $a = 14.3678(7)$ Å, $b = 4.0173(2)$ Å, and $c = 15.8787(7)$ Å. The hydrogen is accommodated in tetrahedral yttrium cavities generated by bending the formerly flat sheets at the trans Y vertices. A higher hydride version also exists. Band structure calculations confirm the 2D metal-bonded character of the compounds and also help illustrate the bonding/matrix changes that accompany the bonding of hydrogen. The ternary structures for both $Y_5M_2Te_2$ and $Sc_5Ni_2Te_2$ can be derived from that of Gd_3MnI_3, the group illustrating three different kinds of metal chain condensation.

Introduction

The understanding of metal−metal bonding and its consequences has experienced much growth since the early empirical studies on metals by Pauling.[1] We have focused considerable attention on the chemistry of the metal-rich halides and chalcogenides of the early-transition metals and have uncovered many different expressions of metal−metal bonding and their import. Examples of new binary group III chalcogenides include Sc_2Te[2] and Dy_2Te,[3] $(Sc,Y)_8Te_3$,[4] Sc_9Te_2,[5] and Lu_8Te[6] whereas contrasting representatives from the complementary binary halides include Sc_7Cl_{10},[7] Y_2Cl_3,[8] and LaI.[9] These chalcogenide and halide compounds share one similar feature: each contains chains of trans-edge-sharing metal octahedra that are further linked via vertices or edges to form diverse 1D, 2D, or 3D metal-bonded structures. The metal halide clusters have relatively more nonmetal anions, and the structures naturally tend to be less condensed. Close structural relationships of these with chalcogenides of later, electron-richer binary systems have been found, such as between Sc_8Te_3 and Ti_8Ch_3[10,11] (Ch = S, Se), or Sc_2Te and Zr_2Te.[12] Later transition metals centered in early transition metal clusters have long been known to stabilize new halide compounds,[13] and comparable research in ternary chalcogenide chemistry has uncovered further structural inter-relationships between $Sc_5Ni_2Te_2$,[14] Gd_3MnI_3,[15] and $Hf_5Co_{1+x}P_{3-x}$, $(0 < x < 0.5)$.[16] These connections have helped us to assess how anion sizes and metal/electron and metal/nonmetal proportions influence structural features.

* To whom correspondence should be addressed. E-mail: jcorbett@iastate.edu.

(1) Pauling, L. *Phys. Rev.* **1938**, *54*, 899. Pauling L. *The Nature of the Chemical Bond*; Cornell University Press: Ithaca, NY, 1960; Chapter 11.
(2) Maggard, P. A.; Corbett, J. D. *Angew. Chem., Int. Ed. Engl.* **1997**, *36*, 1974.
(3) Herle, P. S., Corbett, J. D. *Inorg. Chem.* **2001**, *40*, 1858.
(4) Maggard, P. A.; Corbett, J. D. *Inorg. Chem.* **1998**, *37*, 814.
(5) Maggard, P. A.; Corbett, J. D. *J. Am. Chem. Soc.* **2000**, *122*, 838.
(6) Chen, L.; Corbett, J. D. *J. Am. Chem. Soc.* **2003**, *125*, 7794.
(7) Poeppelmeier, K. R.; Corbett, J. D. *Inorg. Chem.* **1977**, *16*, 1107.
(8) Mattausch, J. B.; Hendricks, J. B.; Eger, R.; Corbett, J. D.; Simon, A. *Inorg. Chem.* **1980**, *19*, 2128.
(9) Martin, J. D.; Corbett, J. D. *Angew. Chem., Int. Ed. Engl.* **1995**, *34*, 233.
(10) Owens, J. P.; Franzen, H. F. *Acta Crystallogr.* **1974**, *B30*, 427.
(11) Weirich, T. E.; Pöttgen, R.; Simon, A. *Z. Kristallogr.* **1996**, *211*, 929.
(12) Örlygsson, G.; Harbrecht, B. *Inorg. Chem.* **1999**, *38*, 3377.
(13) Corbett, J. D. *J. Alloys Compd.* **1995**, *229*, 10.
(14) Maggard, P. A.; Corbett, J. D. *Inorg. Chem.* **1999**, *38*, 1945.
(15) Ebihara, M.; Martin J. D.; Corbett, J. D. *Inorg. Chem.* **1994**, *33*, 2078.
(16) Kleinke, H.; Franzen, H. F. *J. Alloys Compd.* **1996**, *238*, 68; **1997**, *255*, 110.

10.1021/ic0303136 CCC: $27.50
Published on Web 03/26/2004

A new linkage in cluster condensation among the bimetallic layered compounds is reported here for $Y_5M_2Te_2$ (M = Fe, Co, Ni), which also show close electronic and structural interrelationships with Gd_3MnI_3 and $Sc_5Ni_2Te_2$. These features give us further clues as to factors that contribute to the dimensionality and persistent features of metal−metal bonding. (A brief report on these connections has appeared earlier.[17])

From another perspective, compounds between early and late transition metals in binary systems have been found to be important as hydrogen storage materials, $LaNi_5$, for example.[18] The Y−M (M = Fe, Co, Ni) systems among these have also been considered to be very promising for this purpose[19] because of yttrium's lower atomic mass, and YNi_3 does in fact absorb more hydrogen (by weight) than does $LaNi_5$.[20] The phases YNi_2, Y_2Ni_7, and YNi_3 have been studied earlier as hydrogen storage materials, and all are reported to keep their respective structure types, even with up to four bound hydrogen atoms per formula unit.[19] We report here the hydrogen absorption within a different matrix, the 2D Y−Ni layers of $Y_5Ni_2Te_2$, and the resulting structural and bonding transformations.

Experimental Section

Syntheses. All materials were handled in a He-filled glovebox. The material sources (yttrium sheets, iron chunks, cobalt, nickel, and tellurium powder, all with reported purities of >99.9%), and the preparation of Y_2Te_3, have been described before.[4,14]

$Y_5M_2Te_2$ (M = Fe, Co, Ni). Appropriate amounts of the elements and Y_2Te_3 to yield a $Y_5M_2Te_2$ (M = Fe, Co, Ni) stoichiometry (~300 mg total) were pelletized with the aid of a hydraulic press and sealed inside tantalum tubing. The containers were heated to 1050 °C for 84 h inside fused-silica containers and then allowed to cool radiatively inside the furnace. Guinier powder patterns at this point revealed yields from 75 to 95% $Y_5M_2Te_2$ for ~20 reactions, with small amounts of yttrium metal (visual), YTe, and the corresponding late transition metal as impurities. The new products are stable in air for 1−2 weeks as judged visually.

$Y_5Ni_2Te_2H_x$. This compound was initially synthesized via an adventitious hydrogen contamination in newly prepared yttrium powder. A yttrium rod had been hydrided by slowly heating (~10 °C/h) it in a fused-silica apparatus under a hydrogen pressure of 0.8 atm to 700 °C, kept there for 5 h, and allowed to cool radiatively in the furnace. The sample was powderized in an alumina mortar, and Guinier patterns taken at this point revealed a mixture of YH_2 and YH_3. A pure sample of YH_3 was later prepared according to the known *P*−*T*−*C* diagram[21] by reacting a similar mixture under 1 atm of H_2 at 200 °C for 36 h. To prepare granular yttrium metal, the former powdered hydride was dehydrided by heating it in a high-temperature vacuum furnace to 750 °C for 48 h until the pressure decreased to 3×10^{-8} atm. Apparently, the yttrium was not completely dehydrided under the above conditions, although it had started to sinter.

Table 1. Lattice Parameters for the $Y_5M_2Te_2$ (*Cmcm*) and $Y_5Ni_2Te_2H_x$ (*Pnma*) Phases for Refined or Loaded Compositions[a]

compound	*a* (Å)	*b* (Å)	*c* (Å)	*V* (Å^3)
$Y_5Fe_2Te_2$	3.9594(3)	15.057(1)	15.216(1)	907.1(2)
$Y_5Co_2Te_2$	3.9421(6)	15.092(2)	15.021(2)	893.7(4)
$Y_5Ni_2Te_2$	3.977(1)	15.035(2)	14.857(3)	888.4(5)
$Y_5Ni_2Te_2H_x$[b]	14.356(2)	4.0209(3)	15.857(1)	915.3(1)
$Y_5Ni_2Te_2D_x$[c]	14.3678(7)	4.0173(2)	15.8787(7)	916.50(9)
$Y_5Ni_2Te_2D_{0.41(1)}$[d]	14.3282(2)	4.01167(5)	15.8359(2)	910.25(2)
Loaded Compositions				
$Y_5Fe_2Te_2H_2$	3.958(1)	15.058(6)	15.214(7)	906.7(6)
$Y_5Co_2Te_2H_2$	3.942(2)	15.090(5)	15.020(4)	893.4(5)
$Y_5Ni_2Te_2H_{0.4}$[e]	14.359(4)	4.020(1)	15.858(3)	915.5(4)
$Y_5Ni_2Te_2H_{0.6}$	14.353(1)	4.0213(4)	15.853(1)	915.0(1)
$Y_5Ni_2Te_2H_{0.8}$	14.354(3)	4.0163(7)	15.866(2)	914.7(3)
$Y_5Ni_2Te_2H_{1.0}$	14.364(1)	4.0172(4)	15.880(1)	916.4(1)
$Y_5Ni_2Te_2H_{2.0}$	14.352(1)	4.0132(5)	15.876(1)	914.4(2)
$Y_5Ni_2Te_2H_{3.0}$	14.368(1)	4.0302(4)	15.951(1)	923.7(1)
$Y_5Ni_2Te_2H_{4.0}$	14.369(2)	4.0327(5)	15.951(2)	924.3(2)

[a] Guinier powder diffraction data at 23 °C. [b] Sample used in the X-ray single crystal structure determination. [c] From X-ray powder diffraction at 23 °C. [d] From neutron powder diffraction data at −259 °C. [e] All hydrides, with the unit cell transformation to the new space group (**a**, **b**, **c**) → (**b**, **c**, **a**).

Use of this yttrium powder to prepare the $Y_5M_2Te_2$ phases according to the procedure above resulted in an unidentified product for M = Ni. To confirm suspicions about hydride, this product was converted to the known $Y_5Ni_2Te_2$ and then back to the unknown by first heating it to 950 °C for 24 h in the high-temperature vacuum furnace and then allowing it to react at 950 °C with small amounts of YH_3 (in fused silica). The supposed $Y_5Ni_2Te_2H_x$ phase was then prepared from Y_2Te_3, Ni, YH_3, and nonhydrided yttrium sheet as before for the loaded compositions $x = 0.4$, 0.6, 0.8, 1.0, 2.0, 3.0, and 4.0 under the reaction conditions described before for the ternary system. A like reaction was also performed on a 5 g scale with YD_3 at the loaded composition $Y_5Ni_2Te_2D_{1.5}$ for the neutron diffraction data collection. Similar reactions with iron and cobalt (M) instead and loaded as $Y_5M_2Te_2H_2$ gave no evidence of a hydride. All of the pertinent lattice constant data are listed in Table 1.

Powder X-ray Diffraction. The powder diffraction patterns of all phases were obtained with the aid of an Enraf-Nonius 552 Guinier powder camera and monochromatic Cu Kα_1 radiation. The samples were crushed into powder form, mixed with standard silicon (NIST), and placed between two strips of Scotch-brand tape on a frame for mounting on the camera rotation motor. Lattice parameters were obtained by least squares refinements of the measured and indexed lines referenced to silicon.

Single Crystal Diffraction. $Y_5Fe_2Te_2$. Several black, irregularly shaped crystals from reactions loaded as $Y_5Fe_2Te_2$ were mounted inside 0.3 mm i.d. glass capillaries that were sealed off and affixed to metal pins. Their crystal quality was checked by means of Laue photographs, and the best crystal was selected for data collection on a Rigaku AFC6R rotating-anode diffractometer (Mo Kα radiation, graphite monochromator) at 23 °C. The 25 reflections were located from a random search, centered, and used to determine provisional lattice constants, the crystal system, and an orientation matrix. Four octants of data were collected (h, $\pm k$, $\pm l$) to $2\theta_{max} = 56°$ and corrected for Lorentz and polarization effects. The data were further corrected for absorption with the aid of three ψ-scans and, subsequently, with DIFABS (rel transm coeff range: 0.48−1.43). Of 3106 measured reflections, 305 were unique and observed ($I > 3\sigma_I$). Extinction conditions and statistical evidence for centricity indicated one possible space group, *Cmcm*. The structure was solved

(17) Maggard, P. A.; Corbett, J. D. *J. Am. Chem. Soc.* **2000**, *122*, 10740.
(18) Furrer, A.; Fischer, P.; Hälg, W.; Schlapbach, L. *Hydrides for Energy Storage, Proceedings of an International Symposium*; Norway, 1977.
(19) Burnasheva, V. V.; Tarasov, B. P. *Russ. J. Inorg. Chem.* **1984**, *29*, 651.
(20) van Essen, R. H.; Buschow, K. H. J. *J. Less-Common Met.* **1980**, *70*, 189.
(21) Lundin, C. E.; Blackledge, J. P. *J. Electrochem Soc.* **1962**, *109*, 838.

Table 2. Single Crystal X-ray Data Collection and Refinement Parameters for $Y_5Fe_2Te_2$ (First Value) and $Y_5Ni_2Te_2H_x$ (Second Value)

fw	811.42, 817.12
cryst syst[a]	orthorhombic
space group, Z	*Cmcm* (No. 63), 4; *Pnma* (No. 62), 4
ρ_{calcd}, g/cm^3	5.976, 5.897
μ(Mo Kα), cm^{-1}	41.42, 41.26
$R(F_o)$, R_w;[b] $R(F_o^2)$ wR2[c]	4.6, 4.2; 3.4, 7.8

[a] Lattice parameters in Table 1. [b] $R = \sum||F_o| - |F_c||/\sum|F_o|$; $R_w = [\sum w(|F_o| - |F_c|)^2/\sum w(F_o)^2]^{1/2}$, $w = 1/\sigma^2$. [c] $R = \sum|F_o^2 - F_c^2|/\sum F_o^2$; $R_w = [\sum w((F_o^2 - F_c^2)^2/\sum wF_o^2)^2]^{1/2}$, $w = 1/\sigma^2$.

Table 3. Positional and Isotropic-Equivalent Displacement Parameters for $Y_5Fe_2Te_2$, 23 °C

atom[a]	y	z	B_{eq}[b] (Å^2)
Te1	0.3831(2)	0.5388(3)	0.89(7)
Y1	0.0369(2)	0.6187(2)	0.9(1)
Y2	0.2556(2)	0.3750(2)	1.0(1)
Y3	0.6061(3)	$^1/_4$	1.0(2)
Fe1	0.4034(4)	$^1/_4$	1.0(3)
Fe2	0.8263(5)	$^1/_4$	1.0(2)

[a] All atoms on m or $m2m$ with $x = 0$. [b] $B_{eq} = (8\pi^2/3)\sum_i\sum_j U_{ij}a_i^*a_j^*\vec{a}_i\,\vec{a}_j$.

by direct methods (SHELXS[22]) and refined with the package TEXSAN[23] in this space group. The final anisotropic refinement converged at $R(F)/R_w = 4.6/4.2\%$ for the composition $Y_5Fe_2Te_2$. Some data for these processes are given in Table 2, and the atomic positions and isotropic-equivalent displacement parameters are given in Table 3. Additional data collection and refinement parameters, the anisotropic displacement parameters, and a complete distance list are in the Supporting Information.

$Y_5Ni_2Te_2H_x$. Black crystals (of irregular habit) from the reaction loaded as $Y_5Ni_2Te_2H$ were mounted and checked, and the best was taken for a data set collection on a Bruker CCD diffractometer operating at room temperature with Mo Kα radiation. The 90 reflection frames collected with 30-s exposures were analyzed and yielded an orthorhombic unit cell and provisional lattice parameters. One sphere of reflections was collected ($\pm h$, $\pm k$, $\pm l$) to $2\theta_{max} = 56°$, and, when integrated and filtered with SAINTPLUS,[24] these gave 7740 reflections, of which 784 were unique and observed ($I > 3\sigma_I$). An absorption correction was applied with the program package SADABS (rel transm coeff range: 0.73−1.69).[25] Extinction conditions and statistical evidence for centricity indicated one possible space group, *Pnma*, a subgroup of *Cmcm*, and the heavy atom model was obtained and successfully refined with the SHELXTL[22] program. Some data collection and refinement parameters are given in Table 2. The refinement converged at R1/wR2 = 3.4/7.8% for the composition $Y_5Ni_2Te_2$. The hydrogen positions could not be deduced. The positional and isotropic-equivalent displacement parameters for the heavy atoms are given in Table 3. Additional data are available as described above.

Neutron Powder Diffraction. Atomic positions and isotropic displacement parameters for the deuteride $Y_5Ni_2Te_2D_{0.41(1)}$ were established with the aid of neutron powder diffraction data collected at −259 °C on the General Purpose Powder Diffractometer (GPPD) at the Intense Pulsed Neutron Source (IPNS) facility at Argonne National Laboratory.[26] The GPPD is a time-of-flight diffractometer with multidetector arrays at fixed scattering angles, and the high-resolution data from the $2\theta = 90.0°$ and 145.9° detector banks were used. The powder data were refined using the Rietveld method[27] with the PC version of the General Structure Analysis System (GSAS),[28] starting with the fractional coordinate data from the single crystal X-ray study. The final refinement included data in the range $0.6 < d < 3.0$ Å.

Table 4. Powder Neutron Data Collection and Refinement Parameters for $Y_5Ni_2Te_2D_{0.41(1)}$

fw	817.99
space group, Z	*Pnma* (No. 62), 4
temp (°C)	−259
d_{calcd} (g/cm^3)	5.969
no. data	8486
no. reflns (fitted)	3707
variables	72
residuals; R_p, R_{wp}[a] (%)	3.19, 4.59
χ^2	3.509
scattering lengths[b] (10^{-12} cm)	Y, 0.775 Ni, 1.030 Te, 0.580 D, 0.667

[a] $R_p = [\sum(|I_o - I_c|)/\sum I_o]$; $R_{wp} = [\sum(I_o - I_c)^2/\sum wI_o^2]^{1/2}$. [b] Reference 28.

The heavy-atom structural model determined from X-ray diffraction readily refined, and the data also revealed a single deuterium position in a yttrium tetrahedral interstice. Refinement of the occupancy of this position gave 41.1(1)%, with no significant coupling with its displacement parameter. Three impurity phases, YTe, YNi, and YD_2, were also observed and refined to the relative amounts of 13.0(1)%, 7.8(1)%, and 1.28(9)% (by weight), respectively. The background function was a cosine Fourier series with six coefficients, and the final conventional agreement indices were $R_p/R_{wp} = 3.2/4.6\%$ with a reduced χ^2 of 3.509. Some neutron data collection and refinement parameters are listed in Table 4. The neutron diffraction patterns in Figure 1 show the raw intensity data and, from top to bottom in each range, the background, and the individual contributions from the main $Y_5Ni_2Te_2D_{0.41(1)}$ and impurity phases, and the difference between the calculated and observed intensity profiles. Each profile includes tick marks to show the locations of the calculated reflections. The positional parameters from both the X-ray single crystal refinement and the neutron powder diffraction study together with isotropic-equivalent displacement parameters for both are in Table 5. A full distance list is available in the Supporting Information.

Band Calculations. Extended Hückel band calculations were carried out within the tight-binding approximation[29] at 96 k-points spread out over the irreducible wedge for the full structures of $Y_5Fe_2Te_2$ and $Y_5Ni_2Te_2D_1$, the latter at full occupancy after removal of two well-separated D per unit cell. H_{ii} parameters (eV) were Y 5s, −6.61; 5p, −4.18; 4d, −6.27. Fe 4s, −6.20; 4p, −3.00; 3d, −7.97. Ni 4s, −6.62; 4p, −3.19; 3d, −9.44. Te 5s, −21.20; 5p, −12.00;[2] D 1s, −13.60. The data employed for Y, Ni, and Fe were obtained after iteration to charge consistency for the respective structures.

Results and Discussion

Syntheses. Syntheses of the ternary $Y_5M_2Te_2$ (M = Fe, Co, Ni) phases were straightforward, and their lattice

(22) Sheldrick, M. *SHELXS-86*; Universität Göttingen: Göttingen, Germany, 1986.
(23) *TEXSAN*, version 6.0; Molecular Structure Corp.: The Woodlands, TX, 1990.
(24) *SAINTPLUS*; Bruker AXS, Inc.: Madison, WI, 1996.
(25) Blessing, R. H. *Acta Crystallogr.* **1995**, *A51*, 33.
(26) Jorgensen, J. D.; Faber, J., Jr.; Carpenter, J. M.; Crawford, R. K.; Haumann, J. R.; Hitterman, R. L.; Kleb, R.; Ostrowski, G. E.; Rotella, F. J.; Worlton, T. G. *J. Appl. Crystallogr.* **1989**, *22*, 321.
(27) Rietveld, H. M. *Acta Crystallogr.* **1967**, *22*, 151.
(28) Larson, A. C.; Von Dreele, R. B. *General Structure Analysis System*; Report LAUR 86-748; Los Alamos National Laboratory: Los Alamos, NM, 1995.
(29) Hoffmann, R. *J. Chem. Phys.* **1963**, *39*, 1397. Whangbo, M.; Hoffmann, R. *J. Am. Chem. Soc.* **1978**, *100*, 6093.

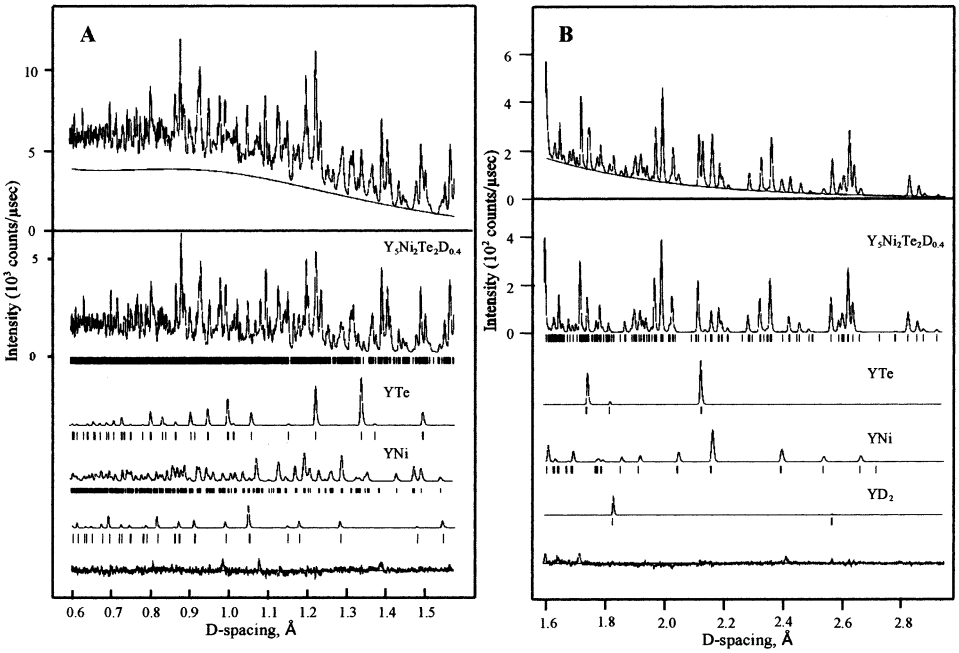

Figure 1. Neutron powder pattern of $Y_5Ni_2Te_2D_{0.41}$ divided into two regions, $d = 0.6-1.6$ Å (A) and 1.6−3.0 Å (B). Shown in each are, from top to bottom, the experimental pattern with fitted background; the calculated patterns for the major and impurity phases, the reflections used (tick marks), and the difference spectrum. Scales are drawn for the experimental and major phases and to define the zero intensities, with all patterns drawn with same scaling.

Table 5. Positional and Isotropic-Equivalent Displacement Parameters from the Single Crystal X-ray Data for $Y_5Ni_2Te_2H_x$ at 23 °C (First Row), and Neutron Powder Data for $Y_5Ni_2Te_2D_{0.41(1)}$ at −259 °C (Second Row)

atom[a]	*x*	*z*	B_{eq}[b] (Å^2)
Te15	0.96613(6)	0.62734(6)	0.85(2)
	0.9659(3)	0.6264(5)	0.27(4)
Te2	0.95423(7)	0.12999(6)	0.94(2)
	0.9552(2)	0.1278(5)	0.27(4)
Y1	0.1489(1)	0.74196(9)	0.84(2)
	0.1483(2)	0.7427(2)	0.23(6)
Y2	0.8864(1)	0.81019(9)	0.86(2)
	0.8857(3)	0.8098(2)	0.26(6)
Y3	0.8823(1)	0.44668(9)	0.94(2)
	0.8816(3)	0.4460(2)	0.38(6)
Y4	0.2079(1)	0.37406(3)	0.91(2)
	0.2071(2)	0.3736(4)	0.28(5)
Y5	0.1376(1)	0.00103(9)	0.93(2)
	0.1392(2)	0.0001(2)	0.28(6)
Ni1	0.7405(1)	0.3218(1)	0.93(3)
	0.7413(2)	0.3217(2)	0.53(5)
Ni2	0.2470(1)	0.5655(1)	1.02(3)
	0.2465(2)	0.5653(2)	0.27(5)
	—	—	—
D	0.2204(6)	0.873(1)	0.9(2)

[a] All atoms on *m*, with $y = 1/4$. [b] $B_{eq} = (8\pi^2/3)\Sigma_i\Sigma_j U_{ij} a_i^* a_j^* \vec{a}_i \vec{a}_j$.

parameters are listed in Table 1. The series of reactions for loaded $Y_5Ni_2Te_2H_x$, $x = 0.4-4.0$, were used as a screen for the possible range of hydrogen absorption into the structure. According to powder diffraction data (lower part of Table 1), the reactions loaded as $Y_5Ni_2Te_2H_x$, $x = 0.4$, 0.6, 0.8, 1.0, 2.0, 3.0, and 4.0, had respective yields of the hydride phase of approximately 85% for the first three and 75%, 60%, 50%, and 30% for the rest. All products contained Y_2Te_3 and YNi impurities, but YH_2 was only observed as a side product at $x = 2.0$ and beyond. The cell volumes for the $x = 0.4-2.0$ series are fairly constant, ∼915 Å^3, whereas those for $x = 3.0-4.0$ distinctly increase to a plateau at ∼924 Å^3. The high yields and lattice dimensions for $x = 0.4-1.0$ imply a single structure type (plus H_2) is present with no detectable trend in lattice constants. The neutron data sample from a reaction loaded as $Y_5Ni_2Te_2D_{1.5}$ refined to a composition of $Y_5Ni_2Te_2D_{0.41(1)}$ and a cell volume consistent with the lower range of *x* (Table 1). A higher hydrogen content with the same heavy atom structure is probable for the reaction products with $x = 3.0-4.0$ with lower % yields. An X-ray single crystal structure determination for the $x = 4.0$ product was attempted, but only consistent unit cell dimensions and crystal system were indicated because of poor crystal quality.

Similar reactions were loaded with iron and cobalt in place of nickel. The lattice constants of reactions loaded $Y_5Fe_2Te_2H_2$ and $Y_5Co_2Te_2H_2$, upper half of Table 1, are statistically unchanged from those for pure $Y_5Fe_2Te_2$ and $Y_5Co_2Te_2$, which implies that no hydride is formed.

Structural Description. $Y_5Fe_2Te_2$. A near-[100] section of the structure viewed along the short 3.95 Å axis is shown in Figure 2, with 99.9% probability thermal ellipsoids. In general, the atom distribution in this view can be described as extended zigzag chains of iron atoms (yellow) along $\vec{a}$ that are sheathed within columns of Y atoms (blue) and further connected via trans-vertices along $\vec{b}$ into 2D metallic layers that are well-separated along $\vec{c}$ by single layers of tellurium atoms (red). The yttrium atoms lie in puckered six-membered rings as they alternate in the projection by $a/2$. A side view in Figure 3 along $\vec{c}$ better illuminates this and the connectivity along $\vec{a}$. The puckered six-members yttrium rings are seen to share atoms along $\vec{a}$ at every vertex.

Selected metal−metal distances for $Y_5Fe_2Te_2$ are listed in Table 6 and marked on the figures. The shortest distance between two Y_5Fe_2 sheets, d(Y1−Y1) = 3.78 Å (Figure 2), corresponds to a weak interaction (below). The shortest

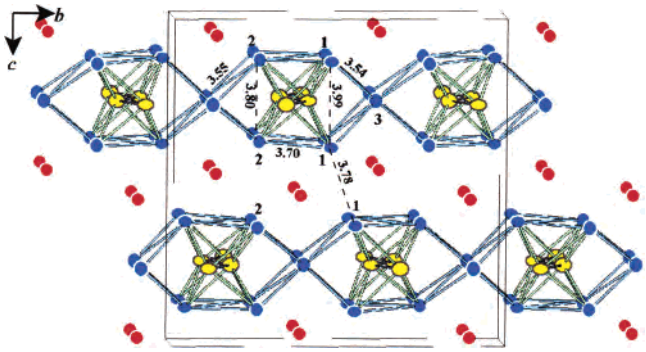

Figure 2. Unit cell of $Y_5M_2Te_2$ (M = Fe, Co, Ni) viewed down the [100] axis, with 99.9% probability displacement ellipsoids. All atoms lie on mirror planes at $x = 0, {}^1/_2$. The marked Y−Y distances (Å) are for M = Fe, with some longer interlayer and intralayer Y−Y distances highlighted with dashed lines. Y, blue; M, yellow; Te, red.

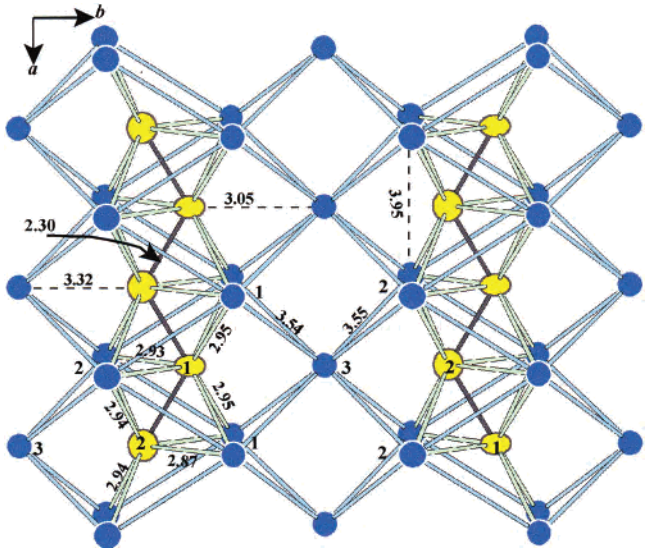

Figure 3. Near-[001] view of a portion of a single infinite Y_5M_2 sheet normal to that in Figure 2. The marked Y−M, M−M, and Y−Y distances in Å are those for M = Fe. Mirror planes lie horizontally through all atoms and in the plane of the page. Y, blue; M, yellow; Te, red.

Table 6. Selected Metal−Metal Distances (Å) and the Corresponding Pairwise Overlap Populations in $Y_5Fe_2Te_2$

atom 1	atom 2	distance	OP	atom 1	atom 2	distance	OP
Y1	Y3	3.543(4)	0.233	Y1	Fe2	2.870(6)	0.287
Y2	Y3	3.551(3)	0.231	Y3	Fe1	3.051(9)	0.278
Y3[a]	Y3	3.9594(3)	0.163	Y2	Fe2	2.944(3)	0.267
Y2[b]	Y2	3.8042(3)	0.160	Y1	Fe1	2.953(3)	0.249
Y1	Y2	3.699(3)	0.108	Y2	Fe1	2.928(6)	0.244
Y1[b]	Y1	3.987(3)	0.107	Y3	Fe2	3.316(9)	0.167
Y1[c]	Y1	3.779(6)	0.051				
Y2[a]	Y2	3.9594(3)	0.044	Fe1	Fe2	2.296(4)	0.289
Y1[a]	Y1	3.9594(3)	0.035				

[a] Short axis repeat. [b] Intralayer distance. [c] Interlayer distance.

yttrium−yttrium distances in the structure are Y3−Y1 and Y3−Y2 at 3.54 and 3.55 Å, respectively, which define elongated body-centered cubes around Y3, the bridging atoms. Alternatively, these cubes (offset by *a*/2) are connected to each other along $\vec{b}$ through long Y1−Y2 bonds at 3.70 Å to form the shell around the iron chain and the bimetallic layer. A related condensation around a late transition-metal chain has been described for $Sc_5Ni_2Te_2$[14] in which pairs of chains built of edge-sharing square-pyramids interconnect to form the sheath. In $Y_5Fe_2Te_2$, the body-centered yttrium cubes may be similarly described as chains of vertex and basal-sharing square pyramids along $\vec{a}$. Longer Y−Y distances, 3.99 and 3.80 Å, occur along $\vec{c}$ as the edges (dashed) of the body-centered cubes (Figure 2). The body-centered cubes form a face-sharing chain along the short *a* axis, 3.95 Å, Figure 3.

The shortest but not particularly remarkable Y−Y distances are just those in the cube around Y3, whereas the remainder of the intrasheet dimensions appear to be governed by strong Y−Fe bonding. Figure 3 shows this more clearly. Each iron atom is surrounded by a trigonal prism of yttrium at distances of 2.87−2.95 Å oriented along $\vec{c}$. For reference, the sum of single bond metallic radii is 2.79 Å.[1] Each face is capped three times, once by Y3 on opposite sides with *d*(Y−Fe) = 3.05 or 3.32 Å and twice by the opposing iron atoms, Fe1 or Fe2, at 2.30 Å. In this arrangement, the capping iron atoms for one trigonal prism are centering atoms for the next on each side, forming interpenetrating trigonal prisms, as in $Sc_5Ni_2Te_2$. Surprisingly, the Fe−Fe chain repeat is a little less than Pauling's single-bond distance, 2.33 Å.[1] This perhaps originates with matrix effects from the strong Y−Fe bonding, as the calculated overlap population per Fe−Fe bond is less than might be expected (below).

The tellurium atoms sandwiched between the bimetallic layers are bound in bicapped trigonal prisms of yttrium, with Y−Te distances of 3.15−3.33 Å, a typical environment for tellurium in these metal-rich phases.[2−4] The shortest Te−Te distance is 3.71 Å (marked), ∼0.15 Å shorter than that normally seen in metal-rich telluride compounds or other van der Waals contacts. This Te−Te distance is evidently determined by both matrix effects and the fact that the Y−Te bonds have some covalency, shrinking the effective Te size. As expected for a metal-rich compound, the Te−Te interaction is calculated to be antibonding (below).

It should be noted that the isostructural $R_5Ni_2Te_2$ phases have also been obtained for R = Gd, Dy according to Guinier powder pattern evidence.[3]

$Y_5Ni_2Te_2D_{0.41(1)}$. The standard setting for the above ternary phase transforms to that for the hydride as (**a**, **b**, **c**) → (**b**, **c**, **a**), and many of the general features are retained. A near-[010] section of the structure in Figure 4 is analogous to that of $Y_5Fe_2Te_2$, Figure 2, and Figure 5 is again the comparable view normal to the sheets. The atom distribution is qualitatively the same, but the bimetallic layers are rumpled to accommodate deuterium (green). Selected distances are in Table 7 and marked in the figures. (The latter show the distances at −259 °C, which are 0.01−0.03 Å less than for the heavy atoms at 23 °C.) The shortest distance between the bimetallic layers, *d*(Y1−Y2) = 3.91 Å (marked), is again a weak interaction. Compared with Y3 in $Y_5Fe_2Te_2$, the equivalent Y4 centers a more distorted cube because of the binding of D, two similarly short yttrium distances, Y5−Y4 at 3.59 Å and Y1−Y4 at 3.55 Å in the bonding environment of D, and two comparably longer distances, Y2−Y4, 3.77 Å, and Y3−Y4, 3.72 Å on the backside. These distorted cubes are connected to another along $\vec{c}$ via Y1−Y3 at 3.62 Å and Y3−Y5 at 3.63 Å and again generate a sheath around

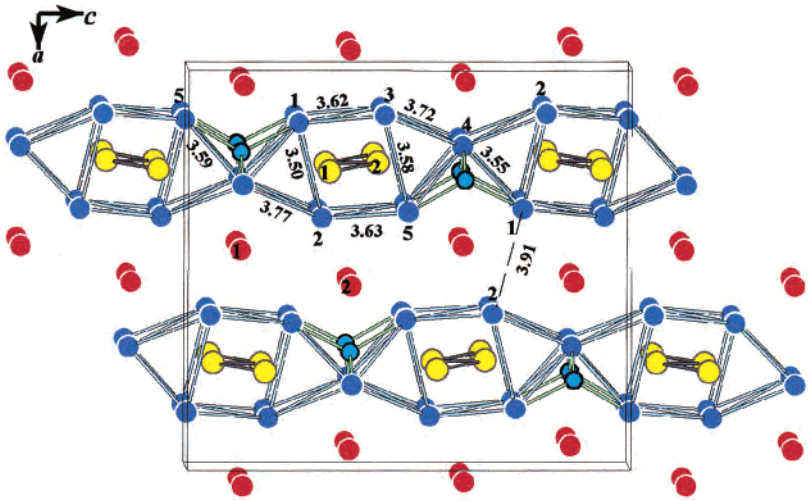

Figure 4. Near-[010] section of the $Y_5Ni_2Te_2D_{0.41(1)}$ unit cell, with Y−Y distances (at −259 °C) labeled in Å. This view is equivalent to that for $Y_5Fe_2Te_2$ in Figure 2. Y, blue; M, yellow; Te, red; D, blue-green.

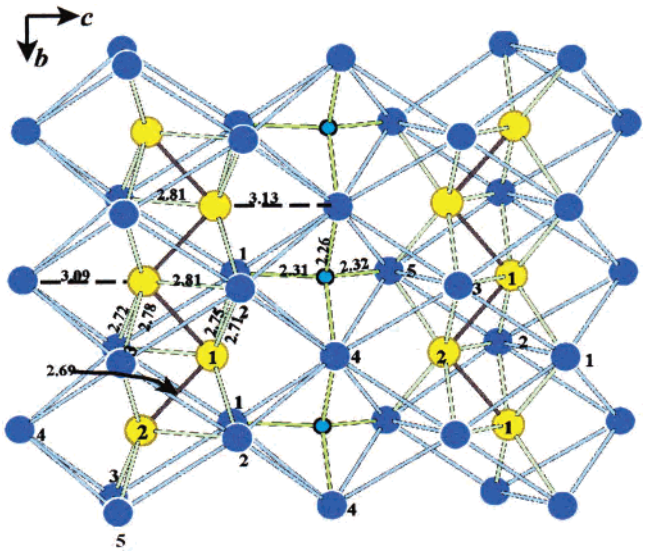

Figure 5. Near-[010] view of the portion of a single sheets in $Y_5Ni_2D_{0.4}$, with Y−Ni, Ni−Ni, and Y−D distances labeled in Å. (Compare Figure 3.) Horizontal mirror planes contain all atoms. Y, blue; Ni, yellow; D, blue-green.

the zigzag nickel chain. The edges across the puckered Y six rings, Y1−Y2 at 3.50 Å and Y3−Y5 at 3.58 Å, are notably ∼0.4 Å shorter than in $Y_5Fe_2Te_2$. These distances reflect the distortion necessary to achieve tetrahedral bonding around D, a smaller interstitial, and a corresponding reapportioning of the metal-based electrons away from Y2−Y4, Y3−Y4 and toward the Y1−Y2, Y3−Y5 edges around D (below).

As seen in Figure 5, each nickel is again surrounded in a distorted trigonal prism of Y along $\vec{a}$ at distances of 2.7−2.8 Å. However, the distances of two Y vertices of the trigonal prism that are also bonded to deuterium have increased: Y1−Ni2, 3.14 Å, and Y5−Ni1, 3.18 Å (not marked). Each nickel trigonal prism is again capped three times, once each by Y4−Ni1 and Y4−Ni2 at 3.13 and 3.09 Å, and twice by opposing Ni1 or Ni2 at 2.69 Å, close to that in $Sc_5Ni_2Te_2$, 2.66 Å.[12] Pauling's single-bond Ni−Ni distance, 2.30 Å,[1] is now much less than observed, and so

Table 7. Selected Metal−Metal Distances (Å) in $Y_5Ni_2Te_2D_{0.41}$ at −259 °C and the Corresponding Pairwise Overlap Populations Calculated for $Y_5Ni_2Te_2D_{1.0}$[a]

atom 1	atom 2	distance	OP	atom 1	atom 2	distance	OP
Y1[b]	Y2	3.502(5)	0.232	Ni1	Y2	2.715(4)	0.237
Y1	Y4	3.552(5)	0.219	Ni2	Y3	2.725(3)	0.234
Y3[b]	Y5	3.577(5)	0.215	Ni1	Y1	2.750(3)	0.231
Y4	Y5	3.590(5)	0.200	Ni2	Y5	2.788(3)	0.219
Y2	Y5	3.634(5)	0.158	Ni1	Y3	2.814(5)	0.207
Y3	Y4	3.715(6)	0.151	Ni2	Y2	2.808(5)	0.206
Y1	Y3	3.624(4)	0.150	Ni2	Y4	3.088(7)	0.127
Y2	Y4	3.772(6)	0.140	Ni1	Y4	3.131(7)	0.116
Y1[c]	Y2	3.910(5)	0.048	Ni2	Y1	3.142(5)	0.107
				Ni1	Y5	3.180(5)	0.102
D	Y4	2.259(4)	0.165				
D	Y1	2.31(2)	0.133	Ni1	Ni2	2.694(2)	0.019
D	Y5	2.32(2)	0.125				

[a] Distances are calculated from the neutron powder diffraction results. Values for *b*-axial repeats are greater than those listed. [b] Intralayer distance. [c] Interlayer distance.

the apparent matrix effects seen in the parent $Y_5Fe_2Te_2$ structure type have disappeared with the bonding of D and the accompanying distortion. The interconnections are still of the same design as before, Figure 3. The added deuterium atom is bound in a yttrium tetrahedron with Y−D distances of 2.26−2.32 Å, a chain of these eclipsed tetrahedra sharing vertices down the *b* axis. The Y−D distances compare well with 2.24 Å for the sum of crystal radii for 6-coordinate Y^{3+} and a general value of 1.10 Å for H^-.[30] Tellurium atoms sandwiched between the bimetallic layers are again bound in a bicapped trigonal prism of yttrium, with Y−Te distances of 3.10−3.32 Å. The closest Te−Te distance is 4.01 Å down the short *b* axis, ∼0.3 Å longer than before.

Theoretical Calculations. Band calculations seemed necessary to understand better the metal−metal bonding in $Y_5Fe_2Te_2$ and $Y_5Ni_2Te_2D_{0.41(1)}$ as conclusions based on just atomic distances alone can be misleading.[2−5] Figures 6 and 7 show the total densities-of-states (DOS) and selected crystal orbital overlap population (COOP) curves for $Y_5Fe_2Te_2$ and $Y_5Ni_2Te_2D_1$, respectively, around E_F. (The change in E_F in the latter because of the refined lower deuterium content is

(30) Corbett, J. D.; Marek, H. S. *Inorg. Chem.* **1983**, *22*, 3194.

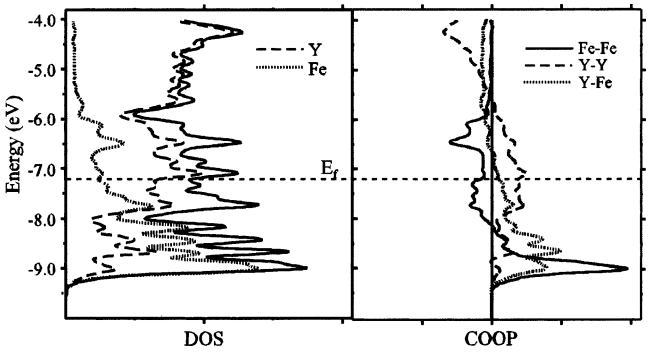

Figure 6. Total densities-of-states (DOS) and crystal orbital overlap population (COOP) curves for $Y_5Fe_2Te_2$. The separate yttrium and iron contributions are projected out in the DOS, and the indicated pairwise interactions, all drawn to the same scale, are shown in the COOP curves.

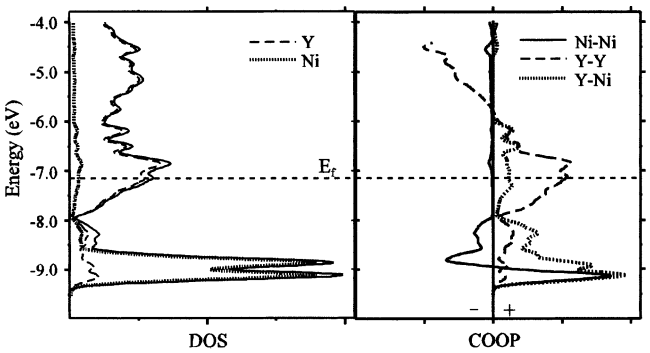

Figure 7. Total densities-of-states (DOS) and crystal orbital overlap population (COOP, right) curves calculated for $Y_5Ni_2Te_2D_{1.0}$. The separate yttrium and nickel contributions are projected out in the DOS data, and the indicated pairwise interactions, all drawn to the same scale, are shown in the COOP curves.

almost imperceptible.) The yttrium and transition metal contributions have each been projected out in the respective DOS.

The Fermi level for the iron ternary resides in a broad conduction band composed of about two-thirds yttrium and one-third iron d-character; hence, the solid is expected to be metallic. Iron is the major contributor to the bands between ~8.0 and −9.0 eV, while yttrium effects lie at higher energies. The COOP curves at the Fermi level reveal Y−Y bonding and Fe−Fe antibonding character to well above E_F, whereas Y−Fe bonding is close to being optimal.

For $Y_5Ni_2Te_2D_1$, the Ni d states naturally lie lower and are more corelike, so the Fermi level falls in a conduction band that is primarily yttrium d, and again, the solid is expected to be metallic. The nickel d-states are much narrower in energy (~1.0 eV) than were the iron states as their energy is about 1.5 eV lower. Now Y−Y and Y−Ni bonding characters persist well above E_f, meaning that the Y−Ni interactions are farther from optimization than Y−Fe in $Y_5Fe_2Te_2$.

Comparison of bond distances with pairwise overlap populations allows one to ascertain where matrix effects, separations that are fixed more by geometric constraints than by bonding effects, appear to be more important. For this purpose, the more important pairwise overlap populations for Y−Y, Y−M, and M−M in $Y_5Fe_2Te_2$ and $Y_5Ni_2Te_2D_1$ are listed in decreasing magnitude along with the distances in Tables 6 and 7. Several irregularities are seen, particularly for the former.

In $Y_5Fe_2Te_2$, the largest Y−Y overlap populations (OPs) occur within the Y3-centered cube, ~0.23 for both Y3−Y1 and Y3−Y2, and also 0.16 along the notably longer repeat distance *a* for Y3−Y3, around which Y−Y bonding dominates. The next largest Y−Y overlap populations include the connection between two cube chains that form the sheath, Y1−Y2 at 0.11, and down the cube edges, Y1−Y1 and Y2−Y2 at 0.11 and 0.16, respectively. The Y1−Y1 interlayer contact is low at 0.051, a weak interaction. The pairwise Y−Fe overlap populations are fairly unstriking, with distances from 2.7 to 3.3 Å that inversely parallel the OP range of 0.29−0.17. The Y3 with more yttrium neighbors also exhibits a large OP, 0.28, for its shortest distance to Fe1 at 3.05 Å. A similar skewing of the environment around the late transition metal was noted in $Sc_5Ni_2Te_2$. (Recall that data for different bond types cannot be intercompared because of the overlap integrals included therein.)

The Fe−Fe contact corresponds to an OP of 0.29, even though its distance is 0.03 Å less than that for an Fe−Fe single bond (Pauling[1]). Its environment is certainly unlike that in elemental iron, and the self-bonding distance is likely to be substantially influenced by strong Fe−Y bonding in what has been called a matrix effect in metal-rich structures.[2−5] The shortest Te−Te interaction, 3.71 Å, has an antibonding OP of −0.033; clearly, this tellurium separation is fixed mainly by the strong Y−Te interactions. The apparently strongest Y−Y bonding (shortest distances) and smallest cell volume (structural compression) of the three new Y_5MTe_2 phases naturally occurs for M = Ni, which may reflect some of the driving force for the hydrogen absorption (below).

In $Y_5Ni_2Te_2D$, the Y−Y pairwise overlap populations (Table 7) parallel inverse variations in distance very much better. The largest deviation on the list, Y1−Y3 at 3.62 Å, exhibits a low OP of 0.15, an expected effect on the basis of its location on the periphery of the metal layer at which a competition with Y−Te bonding occurs. A similar result pertains to the equivalent Y2−Y5. This effective oxidation of external metal-cluster bonds by Te has been seen more clearly before.[5] The shortest, internal Y−Y bonds, Y1−Y2, Y1−Y4, Y3−Y5, and Y4−Y5, all have OP's greater than 0.20. Comparison of these with those for the equivalent separations in $Y_5Fe_2Te_2$ shows that the metal-based electrons have been redistributed away from the equivalent Y3-centered cubes and from the outside of the fold opposite deuterium, (Y4−Y2, Y4−Y3, OP ~ 0.15 vs Y1−Y3, Y2−Y3 in the ternary at ~0.23, respectively) and toward the cube edges (Y1−Y2, Y3−Y5 at ~0.22) and the tetrahedron edges Y1−Y4 and Y4−Y5 (vs Y1−Y1, Y2−Y2 at ~0.16−0.11 respectively). This noticeable change in Y−Y bonding on incorporation of hydrogen may arise from the relative oxidizing effect of hydrogen on the more distant metal atoms.

The Y−Ni pairwise interactions with OPs of 0.24−0.10 neatly parallel decreases in distances over 2.7−3.2 Å with no statistically discernible deviations, in contrast to those for Y−Fe in $Y_5Fe_2Te_2$. The Y−Ni distances in the hydride are ~0.14 Å less than those for Y−Fe. This allows both the

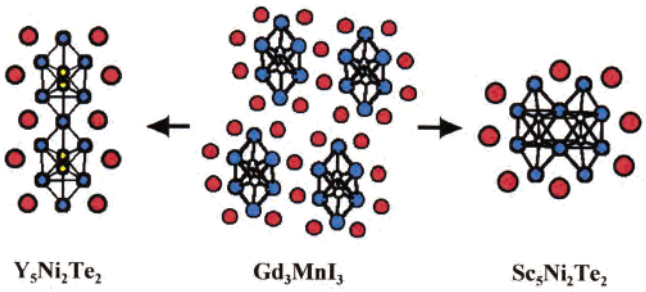

Figure 8. The conceptual transformation of the isolated chains of centered clusters in Gd_3MnI_3 into two $R_5Ni_2Te_2$ structures according to different means of condensation of the cluster chains.

contraction of the yttrium cage around the nickel chain and leaves more electrons available for Y−Y bonding because of the weakness of the Y−Ni bonds in what may be called a cooperative size and valence effect. Last, the Ni−Ni interaction is weak with an OP of only 0.019, and those for Te−Te contacts both down the short *b* axis and between the layers are effectively zero. Matrix effects are clearly less significant here.

Generally, the electronic calculations reveal largely 2D metal-bonded character for both of the title compounds, and Y−M overlap populations that parallel with the corresponding inverse distances well. Hydrogen absorption with a switch to M = Ni seems to diminish compression on the Te−Te and M−M neighbors, and also yields a better correspondence between bond lengths and bond orders for Y−Y and Y−M. The hydrogen absorption effects a redistribution of metal-based electrons away from the neighboring Y−Y bonds.

Structural Comparisons. The present $Y_5M_2Te_2$ phases and the earlier orthorhombic (*Pnma*) $Sc_5Ni_2Te_2$ are, despite their comparable formulas, strikingly different in the nature of their metal−metal aggregation. The columns built of rare-earth-metal six-rings that surround the zigzag chains of the late transition metals in both associate end-on through shared atoms to generate sheets of cluster chains in the former, but only side-by-side in double columns occurs in $Sc_5Ni_2Te_2$. In comparison, the long-known monoclinic Gd_3MnI_3 structure has heretofore represented an isolated and unique architecture seemingly unrelated to any other condensed cluster arrangement. This unusual 1D structure contains isolated single zigzag chains of Mn sheathed by a gadolinium framework that may be traced to substantial distortions of pairs of condensed octahedral chains.[15] We realize now that this remarkable structure can be viewed as a precursor to both of these $R_5M_2Te_2$ structural motifs. Figure 8 illustrates how replacement of the iodine by half as much tellurium in 2 mol of Gd_3MnI_3 (center) together with necessary changes in (transmutations of) the framework (Gd to Y, Sc) and interstitial (Mn to Ni, etc.) atoms and a reductive elimination of 1 mol of RTe leads to observed condensation of the isolated chains in two different ways. That is, on the right part of Figure 8, a Sc_5Ni_2 double chain motif is generated by sharing pairs of metal vertices on the edges of two chains; on the left, a Y_5Ni_2-like motif is formed by sharing of the trans vertices on the original chains. The latter results in the continuous polymerization of parallel Gd_3Mn-like rods into Y_5Ni_2 sheets, whereas the sharing of two vertices on a single edge halts the condensation at the dimer stage in the Sc_5Ni_2 columns. The two products are of course isoelectronic as well. The quasichemical structural change reaction can be written as $2R_3ZI_3 \Rightarrow R_5Z_2Te_2 + RTe$.

A good theoretical approach to this problem quantitatively is not evident to us. However, some energetic differences seem to derive from the two types of products. The first mode affords two more of both Sc−Sc and Sc−Ni bonds whereas the second change provides four more Y−Y bonds. The latter also occurs for $Gd_5Ni_2Te_2$ and Dy_2Ni_2Te.[3] This differentiation follows expectations: R−R bonds between early 4d-bonded transition metals (Y) (or 5d, Ge, Dy) are known to be stronger than for 3d members,[31] whereas the reverse, stronger R−M bonds, favors Sc−M,[32] in both cases the relative bond strengths being inferred from OP analyses.

Progress in the synthesis of low-dimensional metallic phases far exceeds a theoretical predictability, and experiments continue to lead the way.

Conclusions. The $Y_5M_2Te_2$ (M = Fe, Co, Ni) and $Y_5Ni_2Te_2D_{0.41}$ compounds have been synthesized by high-temperature solid-state techniques. Their structures comprise zigzag chains of the late-transition-metal sheathed by yttrium atoms and condensed through trans vertices to form 2D bimetallic layers separated by a single layer of tellurium atoms. Only $Y_5Ni_2Te_2$ is found to absorb hydrogen, which results in a rumpling of the bimetallic sheets through the binding of hydrogen in tetrahedral yttrium cavities. Band structure calculations confirm the largely 2D metal-bonded character of both compounds and show that hydrogen absorption and the change in M reduce the structural compressions in the $Y_5Fe_2Te_2$ structure type. The present orthorhombic structure type derives from Gd_3MnI_3 by a new type of metal condensation that contrasts with another mode recognizable for $Sc_5Ni_2Te_2$.

Acknowledgment. We thank Ilia Guzei for help with the CCD diffractometer. This work was supported by the National Science Foundation, Solid State Chemistry, via Grants DMR-9510278, DMR-9809850, and DMR-0129785, and was carried out in the facilities of the Ames Laboratory, U.S. Department of Energy. The neutron diffraction studies were carried out at Argonne National Laboratory under Contract W-31-109-ENG-38 and with the considerable assistance of Robert W. Henning.

Supporting Information Available: Tables of additional crystallographic and refinement parameters, anisotropic displacement parameters, and a complete listing of nearest neighbor distances. This material is available free of charge via the Internet at http://pubs.acs.org.

IC0303136

(31) Franzen, H. F.; Köckerling, M. *Prog. Solid State Chem.* **1995**, *23*, 265.
(32) Köckerling, M.; Martin, J. D. *Inorg. Chem.* **2001**, *40*, 389.